

Neutron star matter in an effective model

T. K. Jha* , P. K. Raina

Indian Institute of Technology, Kharagpur, India - 721302

P. K. Panda and S. K. Patra

Institute of Physics, Bhubaneswar, India - 751005

(Dated: February 7, 2008)

We study the equation of state (EOS) for dense matter in the core of the compact star with hyperons and calculate the star structure in an effective model in the mean field approach. With varying incompressibility and effective nucleon mass, we analyse the resulting EOS with hyperons in beta equilibrium and its underlying effect on the gross properties of the compact star sequences. The results obtained in our analysis are compared with predictions of other theoretical models and observations. The maximum mass of the compact star lies in the range $1.21 - 1.96 M_{\odot}$ for the different EOS obtained, in the model.

PACS numbers: 21.65.+f, 13.75.Cs, 97.60.Jd, 21.30.Fe, 25.75.-q, 26.60.+c

I. INTRODUCTION

Dense matter studies have opened up new dimensions in understanding the nature and behavioral aspects of nuclear matter at extremes. An ideal laboratory for such studies can be neutron stars, which contains matter around ten times denser than atomic nuclei. These compact stars are believed to be made in the aftermath of type II supernova explosions resulting from the gravitational core collapse of massive stars. All known forces of nature i.e, strong, weak, electromagnetic and gravitational, play key roles in the formation, evolution and the composition of these stars. Thus the study of dense matter not only deals with astrophysical problems such as the evolution of neutron stars, the supernovae mechanism but also reviews the implications from heavy-ion collisions.

Neutron stars are charge neutral, and the fact that charge neutrality drives the stellar matter away from isospin-symmetric nuclear matter, the study of neutron stars lends important clues in understanding the isospin dependence of nuclear forces. Due to β -stability conditions, neutron star is much closer to neutron matter than the symmetric nuclear matter [1]. However, with increasing densities, the fermi energy of the occupied baryon states reaches eigenenergies of other species such as $\Lambda^0(1116)$, $\Sigma^{-,0,+}(1193)$ and $\Xi^{-,0}(1318)$ and the possibility of these hyperonic states are speculated in the dense core of neutron stars ([2]-[4]). Studies on hypernuclei experiments suggests the presence of hyperons in dense matter such as neutron stars. Theoretically also, it has been found that the inclusion of hyperons in neutron star cores lowers the energy and pressure of the system resulting in the lowering of the maximum mass of neutron stars, in the range of observational limits.

Various hadronic models have been applied to describe

the structure of neutron stars. Non-relativistic [5, 6] and relativistic models ([7]-[10]) predict nearly same maximum mass of neutron star. Relativistic models have been successfully applied to study finite nuclei [11] and infinite nuclear matter [12] where they not only satisfy the properties of nuclear matter at saturation but also the extrapolation to high density is automatically causal. Field theories such as the non-linear $\sigma-\omega$ model [13] have been phenomenal in this respect.

Presently we apply an effective hadronic model to study the equation of state (EOS) for neutron star matter in the mean-field type approach [12]. Along with non-linear terms, which ensure reasonable saturation properties of nuclear matter, the model embodies dynamical generation of the vector meson mass that ensures a reasonable incompressibility. Therefore, one of the motivation for the present study is to check the applicability of the model to the study of high density matter. Secondly, the parameter sets of the model are in accordance with recently obtained heavy-ion data [14]. With varying incompressibility and effective nucleon mass the study can impart vital information about their dependency and the underlying effect on the resulting EOS. Also the existing knowledge on the presence of hyperons in the dense core of these compact stars is inadequate, largely because the coupling strength of these hyperons are unknown. So it would be interesting to see the effect of hyperons in the dense core of neutron stars and the predictive power of the present model in establishing the global properties of the resulting neutron star sequences.

The outline of the paper is as follows: First we give a brief description of the ingredients of the hadronic model that we implement in our calculations. After introducing the Tolman-Oppenheimer-Volkov (TOV) equations for the static star, we present some general features of the equation of state and then look at the gross properties of the neutron stars in our calculations and compare our results with the observed masses of the neutron stars, and also with predictions from some of the field-theoretical

tron star mass and radius imposed by recent estimates of the gravitational redshift in the M-R plane. Finally we conclude with outlook on the possible extensions of the current approach.

II. THE EQUATION OF STATE

We start with an effective Lagrangian generalized to include all the baryonic octets interacting through mesons:

$$\begin{aligned} \mathcal{L} = & \bar{\psi}_B \left[(i\gamma_\mu \partial^\mu - g_{\omega B} \gamma_\mu \omega^\mu - \frac{1}{2} g_{\rho B} \vec{\rho}_\mu \cdot \vec{\tau} \gamma^\mu) - g_{\sigma B} (\sigma + i\gamma_5 \vec{\tau} \cdot \vec{\pi}) \right] \psi_B \\ & + \frac{1}{2} (\partial_\mu \vec{\pi} \cdot \partial^\mu \vec{\pi} + \partial_\mu \sigma \partial^\mu \sigma) - \frac{\lambda}{4} (x^2 - x_0^2)^2 - \frac{\lambda B}{6} (x^2 - x_0^2)^3 - \frac{\lambda C}{8} (x^2 - x_0^2)^4 \\ & - \frac{1}{4} F_{\mu\nu} F_{\mu\nu} + \frac{1}{2} g_{\omega B}^2 x^2 \omega_\mu \omega^\mu - \frac{1}{4} \vec{R}_{\mu\nu} \cdot \vec{R}^{\mu\nu} + \frac{1}{2} m_\rho^2 \vec{\rho}_\mu \cdot \vec{\rho}^\mu . \end{aligned} \quad (1)$$

Here $F_{\mu\nu} \equiv \partial_\mu \omega_\nu - \partial_\nu \omega_\mu$ and $x^2 = \vec{\pi}^2 + \sigma^2$, ψ_B is the baryon spinor, $\vec{\pi}$ is the pseudoscalar-isovector pion field, σ is the scalar field. The subscript $B = n, p, \Lambda, \Sigma$ and Ξ , denotes for baryons. The terms in eqn. (1) with the subscript ' B ' should be interpreted as sum over the states of all baryonic octets. In this model for hadronic matter, the baryons interact via the exchange of the σ , ω and ρ -meson. The Lagrangian includes a dynamically generated mass of the isoscalar vector field, ω_μ , that couples to the conserved baryonic current $j_\mu = \bar{\psi}_B \gamma_\mu \psi_B$. In this paper we shall be concerned only with the normal non-pion condensed state of matter, so we take $\vec{\pi} = 0$ and also the pion mass $m_\pi = 0$. The interaction of the scalar and the pseudoscalar mesons with the vector boson generate the mass through the spontaneous breaking of the chiral symmetry. Then the masses of the baryons, scalar and vector mesons, which are generated through x_0 , are respectively given by

$$m_B = g_{\sigma B} x_0, \quad m_\sigma = \sqrt{2\lambda} x_0, \quad m_\omega = g_{\omega B} x_0 . \quad (2)$$

In the above, x_0 is the vacuum expectation value of the σ field, $\lambda = (m_\sigma^2 - m_\pi^2)/(2f_\pi^2)$, with m_π , the pion mass and f_π the pion decay constant, and $g_{\omega B}$ and $g_{\sigma B}$ are the coupling constants for the vector and scalar fields, respectively. In the mean-field treatment we ignore the explicit role of π mesons.

The Dirac equation for baryons is the Euler-Lagrange equation of \mathcal{L} and is obtained as

$$[\gamma_\mu (p^\mu - g_{\omega B} \omega^\mu - \frac{1}{2} g_{\rho B} \vec{\tau} \cdot \vec{\rho}^\mu) - g_{\sigma B} \sigma] \psi_B = 0 . \quad (3)$$

The mass term in the above equation appears in the form $g_{\sigma B} \sigma$, which is referred to as the effective baryon mass, $m_B^* = g_{\sigma B} \sigma$.

We will now proceed to calculate the equation of motion for the scalar field. The scalar field dependent terms from the Lagrangian density are:

$$- \frac{\lambda}{4} (x^2 - x_0^2)^2 - \frac{\lambda B}{6} (x^2 - x_0^2)^3 - \frac{\lambda C}{8} (x^2 - x_0^2)^4 - g_{\sigma B} \bar{\psi}_B \sigma \psi_B + \frac{1}{2} g_{\omega B}^2 x^2 \omega_0^2 , \quad (4)$$

where in the mean-field limit $\omega = \omega_0$. The constant parameters B and C are included in the higher-order self-

values of nuclear matter properties at saturation point. Using equation (2) and $m_B^*/m_B \equiv x/x_0 \equiv Y$, the above

$$-\frac{1}{4}(1-Y^2)^2 + \frac{B}{6c_{\omega B}}(1-Y^2)^3 - \frac{C}{8c_{\omega B}^2}(1-Y^2)^4 + \frac{2g_{\omega B}^2\omega_0^2}{2\lambda x_0^2}Y^2 + \frac{g_{\sigma B}Y}{\lambda x_0^3}\bar{\psi}_B\psi_B \quad (5)$$

Differentiating with respect to Y , we have the equation of motion for the scalar field including all baryons as:

$$\sum_B \left[(1-Y^2) - \frac{B}{c_{\omega B}}(1-Y^2)^2 + \frac{C}{c_{\omega B}^2}(1-Y^2)^3 + \frac{2c_{\sigma B}c_{\omega B}\rho_B^2}{m_B^2Y^4} - \frac{2c_{\sigma B}\rho_{SB}}{m_BY} \right] = 0, \quad (6)$$

where the effective mass of the baryonic species is $m_B^* \equiv Ym_B$ and $c_{\sigma B} \equiv g_{\sigma B}^2/m_\sigma^2$ and $c_{\omega B} \equiv g_{\omega B}^2/m_\omega^2$ are the usual scalar and vector coupling constants respectively. It should be noted that although the term ' λ ' in the Lagrangian does not appear explicitly in eqn. (6), however the effect is there through the mass term, following equation (2) and through x_0 .

For a baryon species, the scalar density (ρ_{SB}) and the baryon density (ρ_B) are,

$$\rho_{SB} = \frac{\gamma}{(2\pi)^3} \int_0^{k_B} \frac{m_B^* d^3k}{\sqrt{k^2 + m_B^{*2}}}, \quad (7)$$

$$\rho_B = \frac{\gamma}{(2\pi)^3} \int_0^{k_B} d^3k, \quad (8)$$

The equation of motion for the ω field is then calculated as

$$\omega_0 = \sum_B \frac{\rho_B}{g_{\omega B}x^2}, \quad (9)$$

The quantity k_B is the Fermi momentum for the baryon and $\gamma = 2$ is the spin degeneracy. Similarly, the equation of motion for the ρ -meson is obtained as:

$$\rho_{03} = \sum_B \frac{g_{\rho B}}{m_\rho^2} I_{3B} \rho_B, \quad (10)$$

where I_{3B} is the 3rd-component of the isospin of each baryon species (given in the Table II).

Traditionally, neutron stars were believed to be composed mostly of neutrons, some of which eventually β -decay until an equilibrium between neutron, proton and electron is reached. The respective chemical potentials

them. Along with charge neutrality condition, $n_p = n_e$, the various particle composition is then determined and the neutron star is believed to be composed of neutrons, protons and electrons. Muons come into picture when $\mu_e = \mu_\mu$, which happens roughly around nuclear matter density, and the charge neutrality condition is altered to $\rho_p = \rho_e + \rho_\mu$. Hyperons can form in neutron star cores when the nucleon chemical potential is large enough to compensate the mass differences between nucleon and hyperons, which happens roughly around two times normal nuclear matter density, when the first species of the hyperon family starts appearing.

The neutron and electron chemical potentials are constrained by the requirements of conservation of total baryon number and the charge neutrality condition given by,

$$\sum_B Q_B \rho_B + \sum_l Q_l \rho_l = 0, \quad (11)$$

with ρ_B and ρ_l are the baryon and lepton densities respectively. These two conditions combine to determine the appearance and concentration of these particles in the dense core of compact objects.

A general expression may be written down for each baryonic chemical potentials (μ_B) in terms of these two independent chemical potentials, i.e., μ_n and μ_e as,

$$\mu_B = \mu_n - Q_B \mu_e \quad (12)$$

where μ_B and Q_B are the chemical potentials and electric charge of the concerned baryon species.

After achieving the solution to these conditions, one obtains the total energy density ε and pressure P for a

$$\begin{aligned} \varepsilon = & \frac{2}{\pi^2} \int_0^{k_B} k^2 dk \sqrt{k^2 + m_B^{*2}} + \frac{m_B^2(1-Y^2)^2}{8c_{\sigma B}} - \frac{m_B^2 B}{12c_{\omega B}c_{\sigma B}}(1-Y^2)^3 \\ & + \frac{m_B^2 C}{16c_{\omega B}^2 c_{\sigma B}}(1-Y^2)^4 + \frac{1}{2Y^2} c_{\omega B} \rho_B^2 + \frac{1}{2} m_\rho^2 \rho_{03}^2 + \frac{1}{\pi^2} \sum_{\lambda=e,\mu^-} \int_0^{k_\lambda} k^2 dk \sqrt{k^2 + m_\lambda^2}, \end{aligned} \quad (13)$$

$$\begin{aligned} P = & \frac{2}{3\pi^2} \int_0^{k_B} \frac{k^4 dk}{\sqrt{k^2 + m_B^{*2}}} - \frac{m_B^2(1-Y^2)^2}{8c_{\sigma B}} + \frac{m_B^2 B}{12c_{\omega B}c_{\sigma B}}(1-Y^2)^3 \\ & - \frac{m_B^2 C}{16c_{\omega B}^2 c_{\sigma B}}(1-Y^2)^4 + \frac{1}{2Y^2} c_{\omega B} \rho_B^2 + \frac{1}{2} m_\rho^2 \rho_{03}^2 + \frac{1}{3\pi^2} \sum_{\lambda=e,\mu^-} \int_0^{k_\lambda} \frac{k^4 dk}{\sqrt{k^2 + m_\lambda^2}} \end{aligned} \quad (14)$$

As explained earlier, the terms in eqns. (13) and (14) with the subscript 'B' should be interpreted as sum over the states of all baryonic octets. The meson field equations ((6), (9) and (10)) are then solved self-consistently at a fixed baryon density to obtain the respective fields along with the requirements of conservation of total baryon number and charge neutrality condition given in equation (12) and the energy and pressure is computed for the neutron star matter. Using the computed EOS for the neutron star sequences, we calculate the properties of neutron stars.

The equations for the structure of a relativistic spherical and static star composed of a perfect fluid were derived from Einstein's equations by Oppenheimer and Volkoff [15]. They are

$$\frac{dp}{dr} = -\frac{G}{r} \frac{[\varepsilon + p][M + 4\pi r^3 p]}{(r - 2GM)}, \quad (15)$$

$$\frac{dM}{dr} = 4\pi r^2 \varepsilon, \quad (16)$$

with G as the gravitational constant and $M(r)$ as the enclosed gravitational mass. We have used $c = 1$. Given an EOS, these equations can be integrated from the origin as an initial value problem for a given choice of central energy density, (ε_c). The value of r ($= R$), where the pressure vanishes defines the surface of the star.

We solve the above equations to study the structural properties of the neutron star, using the EOS derived for the electrically charge neutral hyperon rich dense matter.

III. RESULTS AND DISCUSSION

The parameter set for the present model is listed in Table-1, which is in accordance with recently obtained heavy-ion collision data. With varying effective masses ($m_N^* = 0.8 - 0.9 m_N$) and incompressibility ($K = 210 - 380$ MeV), the study can give us informations on nuclear equation of state and its effect on the prop-

TABLE I: Parameter sets for the model.

set	$c_{\sigma N}$ (fm^2)	$c_{\omega N}$ (fm^2)	B (fm^2)	C (fm^4)	K (MeV)	m_N^*/m_N
I	8.86	1.99	-12.24	-31.59	210	0.85
II	6.79	1.99	-4.32	0.165	300	0.85
III	5.36	1.99	1.13	22.01	380	0.85
IV	8.5	2.71	-9.26	-40.73	300	0.80
V	2.33	1.04	9.59	46.99	300	0.90

TABLE II: Table of baryonic octet

B	Mass (MeV)	Q_B	I_3
p, n	938	1,0	1/2,-1/2
Λ^0	1116	0	0
$\Sigma^{-,0,+}$	1193	-1,0,1	-1,0,1
$\Xi^{-,0}$	1318	-1,0	-1/2,1/2

nuclear saturation properties, E_B , energy per nucleon, -16 MeV at saturation density $0.153 fm^{-3}$, effective nucleon Landau mass $0.8 - 0.9 m_N$, incompressibility, and asymmetry energy coefficient value (≈ 32 MeV), so that our extrapolation to higher density remains meaningful.

We fix the coupling constant $c_{\rho N}$ by requiring that a_{sym} correspond to the empirical value, 32 ± 6 MeV[16]. This gives $c_{\rho N} = 4.66 fm^2$ for $a_{\text{sym}}=32$ MeV.

The baryonic octet under consideration are summarized in Table-2, with their respective masses, charge (Q_B) and isospin (I_3). The electric charge and isospin determine the exact conditions for each hyperon species to appear in the matter. In the absence of any relevant data for hyperon-nucleon or hyperon-hyperon interaction, the understanding of dense matter under these extreme conditions heavily depends on the hypernuclei experiments. The experiment shows bound states of Λ in nuclear medium, although nothing can be said about

In order to include hyperons, one needs to specify the hyperon coupling strength, which is more or less unknown [3, 17]. The EOS at high density is very sensitive to the underlying hyperon couplings, since hyperons are the majority population at high densities and is in turn reflected in the structural properties of the compact stars. The ratio of hyperon to nucleon couplings to the meson fields are not defined by the ground state of nuclear matter, but are chosen on other grounds such as,

(1) Universal coupling scheme (UC): $x_\sigma = x_\omega = 1$, where the hyperons and nucleons couple to the meson fields with equal strength (2) Moszkowski coupling (MC) : $x_\sigma = x_\omega = \sqrt{2/3}$ [18], which is based on the quark sum rule approach and (3) In our present work, we take $x_\sigma = g_{\sigma H}/g_{\sigma N} = 0.7$, $x_\omega = g_{\omega H}/g_{\omega N} = 0.783$ and $x_\omega = x_\rho$, to calculate the EOS for the neutron star matter and gross properties of neutron stars. Here, binding of Λ^0 in nuclear matter: $(B/A)_\Lambda = x_\omega g_{\omega\Lambda} \omega_0 + m_\Lambda^* - m_\Lambda \approx -30$ MeV. However prescription (3) restricts the equation of state of neutron star matter following the constraint of Λ^0 binding in nuclear matter. The choice of $x_\sigma < 0.72$ has been emphasized [19] and also from studies based on hypernuclear levels [20], the choice ($x_\sigma < 0.9$) is bounded from above.

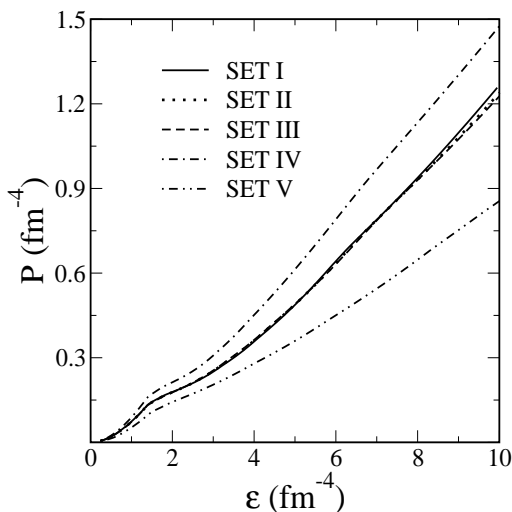


FIG. 1: Equation of state (P vs ε) of neutron star matter with hyperons for the parameter sets listed in Table 1.

The nucleon effective mass and incompressibility strongly influence the EOS of neutron-rich and neutron star matter. Figure 1 displays the equation of state for the five parameter sets. From the figure, it is to be noted that parameter set I, II, and III (with same nucleon effective mass but different incompressibility) follows similar trend upto ten times normal nuclear matter density,

whereas SET IV and V (with different effective mass) deviate from the trend. The difference in incompressibility does not seem to bother much to the resulting equation of state, whereas the difference in effective mass appears to be prominent. However, for all the cases, we find the dip in the curve at $\varepsilon \approx 1.5-2 \text{ fm}^{-4}$, which is the signature of the appearance of first members of the hyperons family namely Λ^0 and Σ^- states.

Similarly, successive appearance of each of the hyperon species contributes to the softening of the EOS. Similar feature is noticeable in most of the other relativistic field theoretical models [21]. Here, it can be seen that a higher effective mass value (Set V) results in a softer EOS and vice-versa, whereas difference in incompressibility is visible at higher densities only.

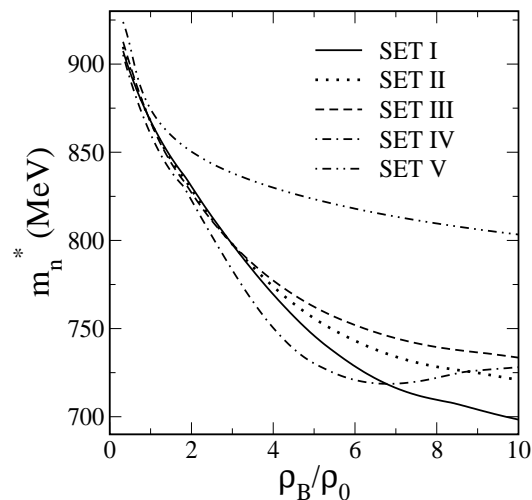


FIG. 2: Effective nucleon mass as a function of baryon density in the neutron star matter upto $10\rho_0$.

The nucleon effective mass ($m_N^* \equiv Y m_N$) as a function of baryon density upto ten times normal nuclear matter density is displayed in figure 2. In case of set I, II and III, the nucleon effective mass follows similar trend, where the nucleon sheds around 22-25 % of its mass in the matter upto $10\rho_0$. Set IV follows the same trend till $6-7\rho_0$ but then the mass increases slowly, the strong repulsive component is responsible for the feature. In case of set V, the nucleon sheds only 15 % of its mass upto ten times nuclear density, but the decrease is rather much slower after a steep decrease till $2\rho_0$. This gradual decrease is as a result of strong scalar component in set V.

To show the sensitivity of EOS to that of the hyperon couplings, we compare in figure 3, EOS corresponding to three different coupling strength for parameter set II. From the figure, it can be seen that Universal coupling

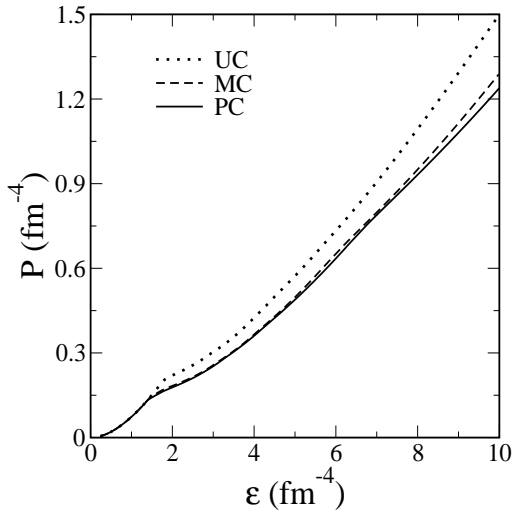


FIG. 3: Equation of state for SET II corresponding to different hyperon coupling schemes, as described in the text.

The coupling strength employed here for the present calculation (PC) is closer to that of MC and is the softest among the three prescriptions. Thus it is conclusive that weaker hyperon coupling leads to softer equation of state because of the underlying weak repulsion in the matter. Similar feature has been noticed in works by Glendening [22] and Ellis et. al [23].

For the sake of completeness we plot in figure 4 the respective particle population of n , p , e and μ^- matter in beta equilibrium upto $10\rho_0$. Muons appear when the chemical potential of the electrons exceeds the rest mass of the muons (106 MeV), which happens roughly at around normal nuclear matter density and becomes one of the particle species in the composition. Consequently the proton fraction increases with appearance of muons in the medium to maintain charge neutrality of the matter. The proton fraction and the electron chemical potential have been found to be important in assessing the cooling rates of neutron stars [24], and the possibility of Kaon condensation in neutron star interiors [25, 26]. We refrain ourselves from further details in this direction.

Figure 5, 6 and 7 displays the relative particle composition of neutron star matter for parameter sets I, II and III with all baryon octets in equilibrium rendering a charge neutral hyperon rich matter. From the plots, it is noteworthy that the difference in the incompressibilities doesn't manifest in the particle composition of the matter very much.

In all three cases, the hyperons start appearing at around $2\rho_0$, where Σ^- appears first, closely followed by Λ^0 . However the former gets saturated because of isospin balance, followed by Λ^0 and Σ^- and then Ξ^- and Σ^0 .

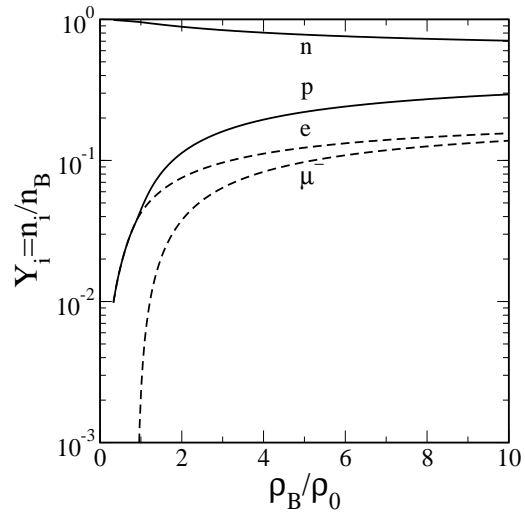


FIG. 4: Relative Particle Population for β -equilibrated matter without hyperons.

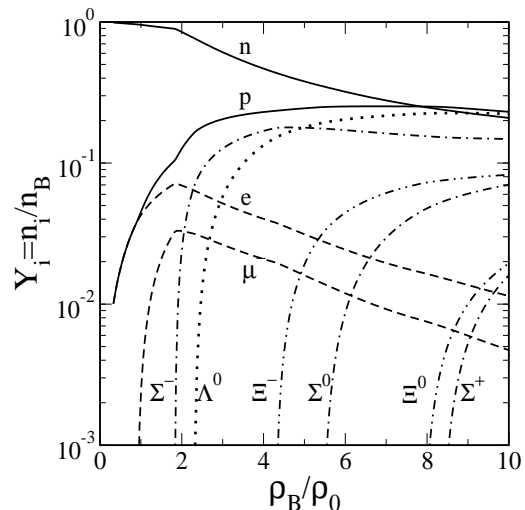


FIG. 5: Relative particle population for neutron star matter with hyperons for parameter Set I ($K=210$ MeV, $m_N^* = 0.85 m_N$).

$4\rho_0$. Λ^0 density further increases with increasing baryon density and is in fact, the dominant particle in the matter composition along with the nucleons. At higher densities other baryon thresholds are attained and they also start appearing. Only noticeable difference in the three cases is the relative population of the hyperons at the

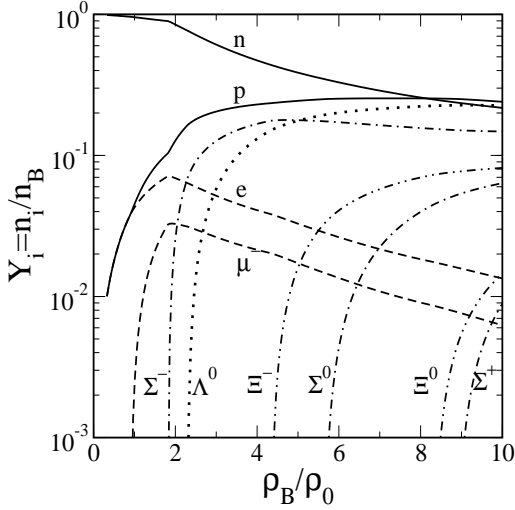


FIG. 6: Relative particle population for neutron star matter with hyperons for Set II ($K=300$ MeV, $m_N^*=0.85 m_N$).

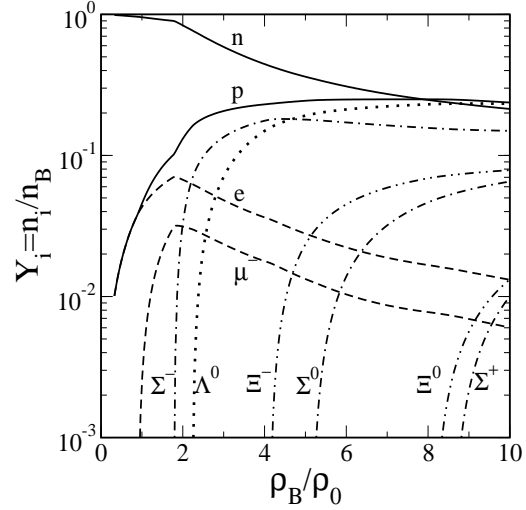


FIG. 8: Relative particle population for the neutron star matter with hyperons for Set IV ($K=300$ MeV, $m_N^*=0.80 m_N$).

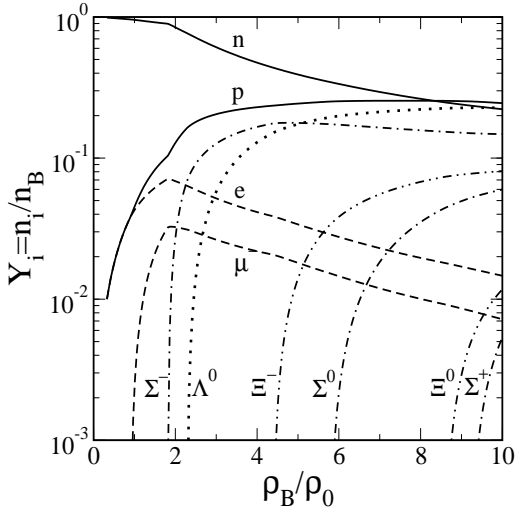


FIG. 7: Relative particle population for neutron star matter with hyperons for Set III ($K=380$ MeV, $m_N^*=0.85 m_N$).

namely Ξ^0 and Σ^+ states. With increasing incompressibility the density at which they appear is pushed further and the population of these states decreases accordingly, although not appreciably.

Similarly figure 8 and figure 9 display the relative particle population for parameter set IV and V respectively.

The difference in effective mass is very much pronounced and is reflected in the respective particle composition of the neutron star matter. The matter composition in case of set IV is more or less similar to first three sets, except that the deleptonisation occurs rather differently. Set V don't predict the presence of Σ^+ state even upto $10\rho_0$. In fact, all the hyperon species seem to appear at relatively higher density than in case of set IV. For example, Σ^0 state appears around $7.5\rho_0$ in case of set V whereas set IV predicts that same at around $5.3\rho_0$. Due to the high effective mass value of set V, the hyperons don't seem to enjoy the previlage of being the dominant species in par with nucleons in the matter as in case of other parameter sets. Even at $10\rho_0$ nucleons comprise $\approx 52\%$ of the total matter.

However for all the five cases, the negatively charged particles are found to be highly favored species in dense matter as evident from their respective order of appearance. At higher density, it can be seen that hyperons forms a sizable population in neutron star matter. They clearly softens the equation of state at high densities. The two independent chemical potentials, μ_n and μ_e along with the charge neutrality condition decides the particle composition. The electron chemical potentials for the five sets are displayed in Figure 10. It can be seen that μ_e follows similar pattern for parameter sets I, II and III, but in case of set IV, it follows similar pattern until $\approx 6\rho_0$ after which it increases again, whereas for set V it starts to decrease after $6\rho_0$.

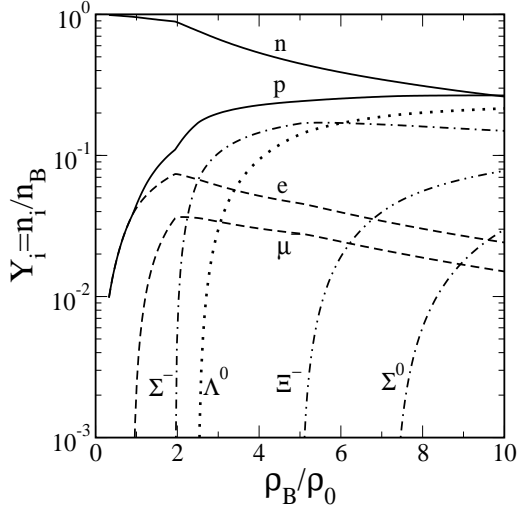


FIG. 9: Relative particle population for the neutron star matter with hyperons for Set V ($K=300$ MeV, $m_N^* = 0.90 m_N$).

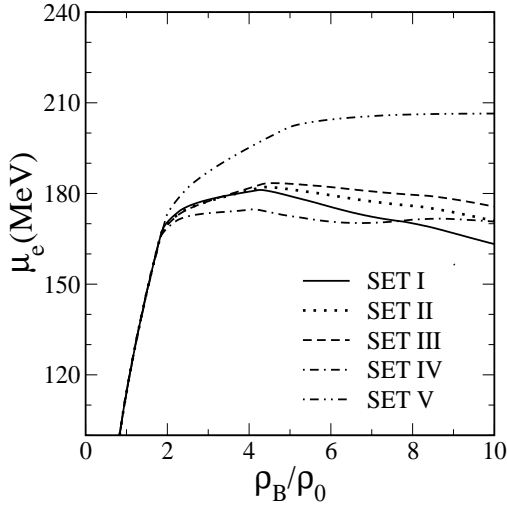


FIG. 10: Electron chemical potential as a function of baryon density upto $10 \rho_0$.

stant. For all the sets at $\approx 2 \rho_0$, we see a sharp turn in the electron potential, where the first charged hyperon species, Σ^- appears. At that point μ_e compensates the mass difference between Σ^- and Λ^0 thereby triggering the appearance of the former. Leptons primarily main-

not predict any charged hyperon species after $\approx 6 \rho_0$, the electron potential remains constant thereafter.

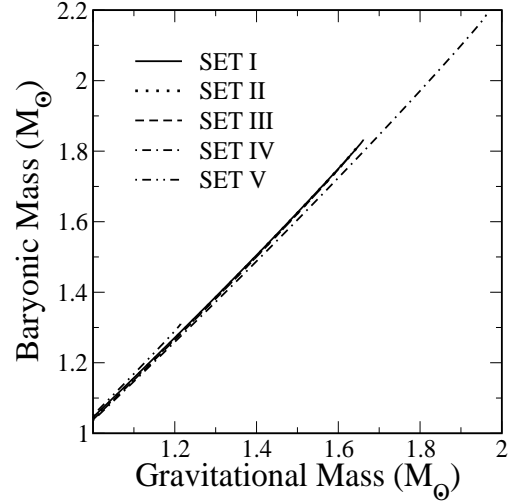


FIG. 11: Baryonic mass (M_\odot) of the star as a function of Maximum mass (M_\odot) for the five sets.

As stated, the properties of neutron star is unique to the EOS considered. Using these EOS, we now calculate some of the global properties of neutron star by solving the TOV equation. Figure 11 shows the maximum baryonic mass M_b (M_\odot) obtained as a function of star mass for the five parameter sets. The curves for set I, II and III coincides with each other, whereas set IV and V are distinctly apart, the reason can be attributed to their different effective mass values. However the baryonic mass always exceeds the gravitational mass, which is typical of compact objects. The difference between the two is defined as the gravitational binding of the star. The baryonic masses obtained for set I, II and III are $1.83M_\odot$, $1.81M_\odot$ and $1.79M_\odot$ respectively. Whereas sets IV (stiff) and V (soft) EOS represents the two extremes among all the parameter sets. The corresponding baryon masses obtained are $2.18M_\odot$ and $1.31M_\odot$.

Gravitational mass of the neutron star as a function of central density of the star is plotted in Figure 12. Stable neutron star configurations are the regions where $\frac{dM}{d\varepsilon_c} > 0$. Beyond the maximum mass, gravity overcomes and results in the collapse of the star. Set I, II and III which vary in incompressibilities predicts almost same central density $\approx 7.9 \times 10^{14} \text{ g cm}^{-3}$ for the star at maximum mass denoted by filled circles in the plot. The maximum mass obtained are $1.66M_\odot$, $1.65M_\odot$ and $1.63M_\odot$ for set I, II and III respectively. Set IV and V predicts the maximum mass to be $1.96M_\odot$ and $1.21M_\odot$ respectively with corresponding central densities $7.7 \times 10^{14} \text{ g cm}^{-3}$ and $9.2 \times 10^{14} \text{ g cm}^{-3}$ respectively. Beyond the maximum mass

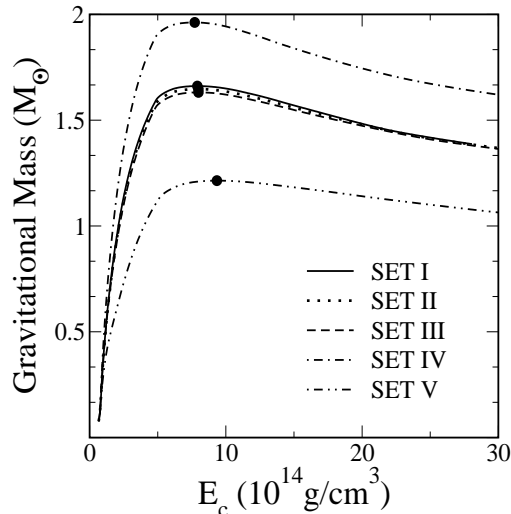


FIG. 12: Maximum mass of the neutron star sequences as a function of central density of the star (in $10^{14} \text{ g cm}^{-3}$).

neutron star masses like $M_{J0751\pm1807} = 2.1 \pm 0.2 M_{\odot}$ [27], $M_{4U1636\pm536} = 2.0 \pm 0.1 M_{\odot}$ [28], $M_{VelaX-1} = 1.86 \pm 0.16 M_{\odot}$ [29] and $M_{VelaX-2} = 1.78 \pm 0.23 M_{\odot}$ [30, 31] predicts massive stars. Our results agrees remarkably with these observed masses except for set V.

Figure 13 displays the maximum mass of the neutron star as a function of the star radius. In order to calculate the radius, we included the results of Baym, Pethick and Sutherland [32] EOS at low baryonic densities. The radius predicted for the sets I, II, and III are ≈ 16.7 km, whereas for set IV and V, it comes out to be 17.43 and 15 km respectively. It is to be noted that in the relativistic regime, the maximum masses obtained by the non-linear walecka model (NLWM) and the quark-meson coupling model [33] are $1.90 M_{\odot}$ and $1.98 M_{\odot}$ respectively. The masses obtained in our calculations are in fair agreement with these calculations. In the relativistic mean field approach the properties of neutron star was studied [9] where it was pointed out that a bigger effective nucleon mass results in a low mass star but with larger radius. Our results lead to the same interpretation.

However because wide range of masses and radius of neutron star being placed by different models, it is therefore important to impose constraints that can put stringent condition in the M-R plane. Constraints on the mass-radius plane can be obtained from accurate measurements of the gravitational redshift of spectral lines produced in neutron star photospheres. Measuring M/R is particularly important to constrain the EOS of dense matter.

Recently a constraint to M-R plane was reported [34]

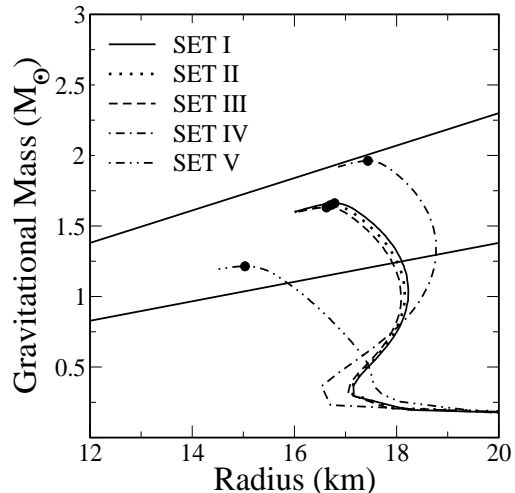


FIG. 13: Maximum mass of the neutron star (in solar mass) as a function of radius (in Km) for the five Sets. The two solid curves corresponds to $M/R = 0.069$ and $M/R = 0.115$. (The solid circles represent the values at maximum mass.)

TABLE III: Properties of Neutron star as predicted by the model

SET	$M(M_{\odot})$	$E_c(10^{14} \text{ g cm}^{-3})$	$R(\text{Km})$	$M_b(M_{\odot})$	Z
I	1.66	7.90	16.78	1.83	0.19
II	1.65	7.99	16.70	1.81	0.19
III	1.63	7.99	16.62	1.79	0.19
IV	1.96	7.72	17.44	2.18	0.22
V	1.21	9.34	15.03	1.31	0.15

the source spectrum of the IE 1207.4-5209 neutron star, which limits $M/R = (0.069 - 0.115) M_{\odot}/\text{km}$. The region enclosed in figure 13 by two solid lines denotes the area enclosed in accordance with the observed range. All the parameter set of the present model satisfies the criterion very well. Another important aspect of compact objects is the observed gravitational redshift, which is given by

$$Z = \frac{1}{\sqrt{1 - 2GM/Rc^2}} \quad (17)$$

The gravitational redshift interpreted by the M/R ratio comes out to be in the range $Z = 0.12 - 0.23$, which is plotted in figure 14. For Set I, II and III, the redshift is nearly same because redshift primarily depends on the mass to radius ratio of the star, which in case of first three sets is nearly same.

For all the parameter sets, the redshift obtained at

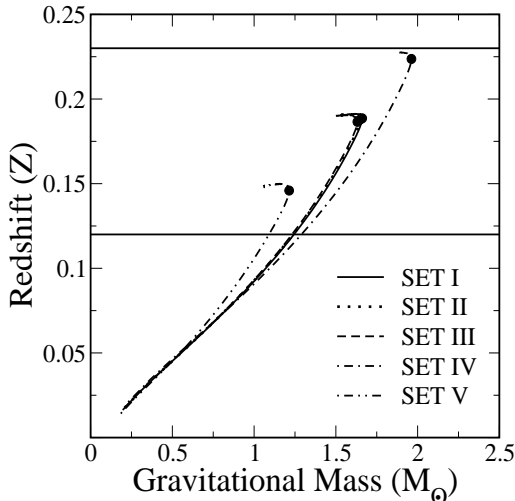


FIG. 14: Gravitational Redshift (Z) as a function of Maximum mass of the neutron star for the five parameter sets. (The solid circles represent the values at maximum mass). The area between solid horizontal lines represents the redshift values $Z = (0.12 - 0.23)$ [34].

responds to $R/M = (8.8 - 14.2)$ km/ M_\odot . Our calculation predicts R/M in the range $(8.90 - 12.40)$ km/ M_\odot , which is consistent with the observed value. The predictive power of the model is evident from figure 14, where we compare the gravitational redshift as a function of the star mass for the five parameter sets. The overall results of our calculation are presented in Table 3.

IV. SUMMARY AND OUTLOOK

We studied the equation of state of high density matter in an effective model and calculated the gross properties for neutron stars like mass, radius, central density and redshift. We analysed five set of parameters with incompressibility values $K=210, 300$ and 380 MeV and effective masses $m^* = 0.80, 0.85$ and $0.90 m_n$, that satisfies the nuclear matter saturation properties. The results are then compared with some recent observations and also a

few field theoretical models. It was found that the difference in nuclear incompressibility is not much reflected in either equation of state or neutron star properties, but nucleon effective masses were quite decisive. At maximum mass, the central density of the star for sets I, II, III and IV was found to be $\approx 3 \rho_{nm}$ (nuclear matter density) but for set V, it was found to be $\approx 3.5 \rho_{nm}$, which has the highest effective mass value. Similarly the maximum mass obtained for the the five EOS lies in the range $1.21-1.96 M_\odot$. Set V, which is softest among all parameter sets, predicts lowest maximum mass $1.21 M_\odot$, whereas set IV (stiff) predicts the maximum mass to be $1.96 M_\odot$ and also is the star with the largest radius. The difference in maximum mass and radius of the star in case of set I, II and III is negligible, and so the predicted redshift comes out nearly same, whereas set IV and V presents the two extremes in overall properties, which is the reflection of their different effective mass values. Overall, mass predicted by all the parameter sets agree well with most of the theoretical work and observational limits.

The results were also found to be in good agreement with recently imposed constrains on neutron star properties in the M-R plane, and the redshift interpreted therein. Further, the precise measurements of mass of both neutron stars in case of PSR B1913+16 [35], PSR B1534+12 [36] and PSR B2127+11C [37] are available which can put constrains on the nuclear equation of state. Masses of neutron stars in X-ray pulsars are also consistent with these values, although are measured less accurately. In case of radii, the values are still unknown, however some estimates are expected in a few years, which would further constrain the EOS of neutron star in the M-R plane. In future, we intend to study the effect of rotation to neutron star structure and also the phase transition aspects in the model. It is worth mentioning that the density-dependent meson-nucleon couplings is very much successful in non-linear Walecka model[38] and similar work in this direction would be interesting.

Acknowledgments

One of us TKJ would like to thank facilities and hospitality provided by Institute of Physics, Bhubaneswar where a major part of the work was done. This work was supported by R/P, under DAE-BRNS, grant no 2003/37/14/BRNS/669.

[1] S.L. Shapiro and S.A. Teukolski, *Black holes, white dwarfs, and Neutron stars* (Wiley, New York, 1983).
[2] N.K. Glendening, Phys. Lett. **B114**, 392 (1982); N. K. Glendening, Astrophys. J. **293**, 470 (1985); N. K. Glendening, Z. Phys. **A 326**, 57 (1987).
[3] M. Prakash, I. Bombaci, M. Prakash, P.J. Ellis, J.M. Lattimer and R. Knorren, Phys. Rep. **280**, 1 (1997).

[4] J. Schaffner-Beilich and I.N. Mishustin, Phys. Rev. **C 53**, 1416 (1996).
[5] A. Akmal, V.R. Pandharipande and D.G. Ravenhall, Phys. Rev. **C 58**, 1804 (1998).
[6] R.B. Wiringa, V. Fiks and A. Fabrocini, Phys. Rev. **C 38**, 1010 (1988).
[7] J.D. Walecka, Ann. Phys. **83**, 491 (1974).

- [8] A. Lang, B. Blatt, W. Cassing, V. Koch, U. Mosel and K. Weber, Z. Phys. **A 340**, 207 (1991).
- [9] N. K. Glendenning, F. Weber and S.A. Moszkowski, Phys. Rev. **C 45**, 844 (1992).
- [10] H. Heiselberg and M. Hjorth-Jensen, Astro. J. Lett. **525**, L45 (1999).
- [11] T. Sil, S.K. Patra, B.K. Sharma, M. Centelles and X. Viñas, Phys. Rev. **C 69**, 044315 (2004); M. Del Estal, M. Centelles, X. Viñas, and S.K. Patra, Phys. Rev. **C 63**, 044321 (2001); S. K. Patra, M. Del Estal, M. Centelles and X. Viñas, Phys. Rev. **C 63**, 024311 (2001).
- [12] P. Arumugam, B.K. Sharma, P.K. Sahu, S. K. Patra, T. Sil, M. Centelles and X. Viñas, Phys. Lett. **B 601**, 51 (2004); P.K. Panda, A. Mishra, J.M. Eisenberg and W. Greiner, Phys. Rev. **C56**, 3134 (1997).
- [13] J. Boguta and A.R. Bodmer, Nucl. Phys. **A 292**, 413 (1977).
- [14] P. Danielewicz, R. Lacey, W.G. Lynch, Science **298**, 1592 (2002).
- [15] J.R. Oppenheimer and G.M. Volkoff, Phys. Rev **55**, 374 (1939); R.C. Tolman, Phys. Rev **55**, 364 (1939).
- [16] P. Möller, W.D. Myers, W.J. Swiatecki and J. Treiner, At. Data Nucl. Data Tables **39**, 225 (1988).
- [17] N.K. Glendenning Phys. Rev. **C 64**, 025801 (2001).
- [18] S.A. Moszkowski, Phys. Rev. **D 9**, 1613 (1974).
- [19] N.K. Glendenning and S.A. Moszkowski, Phys. Rev. Lett. **67**, 2414 (1991).
- [20] M. Rufa, J. Schaffner, J. Maruhn, H. Stocker, W. Greiner and P. G. Reinhard, Phys. Rev. **C 42**, 2469 (1990).
- [21] A. Mishra, P.K. Panda and W. Greiner, J. Phys. **G 28**, 67 (2002).
- [22] N.K. Glendenning, Nucl. Phys. **A 493**, 521 (1989).
- [23] J. Ellis, J.I. Kapusta and K.A. Olive, Nucl. Phys. **B 348**, 345 (1991).
- [24] C.J. Pethick, Rev. Mod. Phys. **64**, 1133 (1992).
- [25] G.E. Brown, C.H. Lee, M. Rho and V. Thorsson, Nucl Phys. **A 567**, 937 (1994).
- [26] V.R. Pandharipande, C.J. Pethick and V. Thorsson, Rev. Lett. **75**, 4567 (1995).
- [27] D.J. Nice, E.M. Spalver, I.H. Stairs, O. Loehmer, A. Jessner, M. Kramer and J.M. Cordes, Astrophys. J. **634** 1242 (2005).
- [28] D. Barret, J.F. Olive and M.C. Miller, *astro-ph/0605486*.
- [29] O. Barziv, L. Kaper, M.H. van Kerkwijk, J.H. Telling and J. van Paradijs, Astron. & Astrophys. **377** 925 (2001).
- [30] J. Casares, P.A. Charles and E. Kuulkers, Astro. J. **493** L39 (1998).
- [31] J.A. Orosz and E. Kuulkers, Mon. Not. R. Astron. Soc. **305** 132 (1999).
- [32] G. Baym, C. Pethick and P. Sutherland, Astrophys. J. **170**, 299 (1971).
- [33] P.K. Panda, D.P. Menezes, C. Providência, Phys.Rev. **C69**, 025207 (2004); P.K. Panda, D.P. Menezes, C. Providência, Phys.Rev. **C69**, 058801 (2004); D.P. Menezes, P.K. Panda and C. Providência, Phys. Rev. **C 72**, 035802 (2005).
- [34] D. Sanyal, G.G. Pavlov, V.E. Zavlin and M.A. Teter, Astrophys. J. **574** L61 (2002).
- [35] J.H. Taylor and J.M. Weisberg, Astrophys. J. **345**, 434 (1989).
- [36] A. Wolszczan, Nature **350**, 688 (1991).
- [37] W.T.S. Deich, S.R. Kulkarni in *Compact Stars in Binaries*, J. van Paradijs, E.P.J. van den Heuvel and E. Kuulkers eds., Dordrecht, Kluwer (1996).
- [38] T. Niksic, D. Vretenar, P. Finelli and P. Ring, Phys. Rev. **C66**, 024306 (2002).